Coupled Systems Mechanics, *Vol. 5, No. 3 (2016) 235–254*
DOI: https://doi.org/10.12989/csm.2016.5.3.235

Strongly coupling partitioned scheme for enhanced added mass computation in 2D fluid-structure interaction

Emmanuel Lefrançois*[1], Anaïs Brandely[1] and Stéphane Mottelet[2]

[1]*Roberval Laboratory CNRS UMR 7337, Université de Technologie de Compiègne - Sorbonne Universités, CS 60319, 60203 Compiègne, France*
[2]*TIMR Laboratory EA 4297, Université de Technologie de Compiègne - Sorbonne Universités, CS 60319, 60203 Compiègne, France*

(Received September 1, 2016, Revised December 2, 2016, Accepted December 17, 2016)

Abstract. A numerical model for fluid-structure interactions (abbr. FSI) is presented in the context of sloshing effects in movable, partially filled tanks to improve understanding of interactions between the fluid and the dynamics of a tank flexibly attached to a vehicle. The purpose of this model is to counteract the penalizing impact of the added mass effect on classical partitioned FSI coupling scheme: the proposed investigation is based on an added mass corrected version of the classical strongly coupled partitioned scheme presented in (Song *et al.* 2013). Results show that this corrected version systematically allows convergence to the coupled solution. In the rare cases where convergence is already obtained, the corrected version significantly reduces the number of iterations required. Finally, it is shown that the convergence limit imposed by added mass effect for the non-corrected coupling scheme, is directly dependent on the aspect ratio of the fluid domain and highly related to the precision order of the temporal discretization scheme.

Keywords: fluid-structure interaction; added mass; sloshing; coupling partitioned scheme

1. Introduction

Among the physical effects resulting from the motion of a fuel tank, *sloshing* is one of the most noticeable and (Ibrahim 2005) is still considered as the best reference. This can be defined as the motion of the free surface of the liquid in a partially filled, moving tank. The sloshing problem has been investigated in numerous significant studies and in a variety of fields, including astronautics (Veldman *et al.* 2007, Chiba *et al.* 2013), civil engineering (Nagashima and Tsukuda 2013, Keivani *et al.* 2014), road transport (Wachowski *et al.* 2010, Raj and *et al.* 2014, Khezzar *et al.* 2009) and naval engineering (Liu and Lin 2009). This paper is essentially concerned by the numerical investigation of *fluid-structure interactions* (abbr. FSI) that may appear between the liquid and the moving and deformable tank and lead to undesirable noises. Numerical simulation of FSI is a way of identifying the noise resulting from fuel sloshing that can reduce the need for very expensive

*Corresponding author, Emmanuel Lefrançois, E-mail: emmanuel.lefrancois@utc.fr

http://www.techno-press.org/?journal=csm&subpage=8 ISSN: 2234-2184(Print), 2234-2192(Online)

experimental tests, but it requires a specific coupling scheme. In this case, it calls for a *partitioned* coupling with a dedicated solver for each of the two physics.

Exchanges take place regularly between the two solvers via a coupling scheme (Felippa *et al.* 2001, Sy and Murea 2012, Wang *et al.* 2012, He 2015) that is based on successive solutions produced by the fluid and structure solvers. The coupling is termed *strongly coupled partitioned* coupling if an iterative procedure is used to ensure convergence of the coupled solution. In an industrial context the biggest advantage of this kind of coupling with regards with the monolothic coupling, is the modularity of the approach, making the different solvers much easier to implement and allowing distributed computation.

The major drawback of the *standard* partitioned FSI coupling scheme is that where higher density fluids are involved (meaning strong effects of added mass (Idelsohn *et al.* 2009, Kassiotis *et al.* 2010)), convergence is no longer guaranteed, and divergence will generally be observed, regardless of the chosen time step for incompressible flows (Fernández *et al.* 2005, van Brummelen 2009). The proposal of a coupling procedure similar to the one exposed in this paper has been proposed and a mathematical and convergence analysis detailed in (Baek and Karniadakis 2012). The idea is to introduce fictitious mass, rigidity and damping matrices that may counteract the added mass effect and better improve the convergence to the solution. However, based on our own experience (Song *et al.* 2013), the added mass matrix may not be reduced to the structure mass matrix ponderated by a density ratio, this point being motivated by strong interactions observed between all the modal components of the structure: the added mass effect must be clearly expressed by a full matrix based on physical considerations.

We should point out that the objective of this paper is not here to develop a complete and best-suited mathematical model for sloshing effects, but to show that the use of a standard FSI scheme will necessarily encounter a limit for convergence due to added mass effect, and this whatever the complexity of the employed codes. For this and convinced that *simplifying is part of the understanding process*, it has been decided to voluntarily reduce the complexity of both solvers (fluid and structure) to firstly point out the convergence limit with regards to added mass effect and secondly to show that a corrected version of the standard partitioned FSI scheme (Song *et al.* 2013) permits to systematically ensure convergence. The selected simplified fluid model is here based on a non-stationary potential approach in 2 dimensions, completed by a condensing free-surface approach to significantly reduce CPU time. Even if a VOF approach may be considered as more efficient (Kassiotis *et al.* 2011), the exposed method (restricted to a linear analysis) combined with a condensation ability (see § 3.2), permits to drastically reduce the global number of *dof* in retaining only the ones attached to the free surface. The flexibility here comes from the mountings attaching the tank to the vehicle, since the tank itself is assumed to be rigid. Particular attention is given to quantifying the effect of additional mass on convergence and on the coupling results.

The present article is divided into five sections, the first being this introduction. In the second section the mathematical models for the example of a partially filled tank (flexibly attached) fully developed so as to enable a numerical analysis. In a third section, proposed numerical models are detailed as well as the standard FSI scheme. The fourth section first presents (§ 4.1) the particular case of a full, closed tank for which the classical FSI scheme systematically fails. The limit value of the mass ratio between the fluid and the tank for avoidance of the divergence effect is predicted and numerically validated using a simple finite element approach. The proposed corrected coupling

scheme based on added mass estimation is then described in detail (§ 4.2). In particular, we show that the divergence effect is avoided irrespective of the fluid density, and the result is validated with the same numerical coupling scheme. In the last part of this section (§ 4.3.2) we apply our proposed approach to cases involving partially filled tanks, where we link the added mass effect to the aspect ratio of the fluid domain. The fifth and final section concludes the paper with current investigations and perspectives.

2. Mathematical models for a partially filled tank

This section describes the different models used to investigate the sloshing effect in a partially filled rectangular tank. The situation is illustrated in Fig. 1(a). Without loss of generality, the analysis is in two dimensions (2D) (Fig. 1(b)). Indeed, experimental measurements in (Brandely and Lefrançois 2016) point to 2D fluid flow behavior for axial sloshing in parallelepipedic tanks whose width b is of the same order as the other two dimensions.

The tank of mass m is assumed to be rigid but flexibly attached to its moving environment (for example, via a flexible mounting on the vehicle or test bench). This flexibility equates to a spring (of rigidity k) attached at one end to a fixed element. The tank's position with respect to its rest position is denoted $u(t)$, and its velocity denoted $\dot{u}(t)$.

The fluid is a liquid (heavy fluid) and defined by its volumic mass ρ. Viscosity effects are here neglected. Its free surface elevation is defined by $\eta(x,t)$.

2.1 Structure model

The tank is governed by the *Fundamental Principle of Dynamics* (FPD). For a movable tank located at $u(t)$ with respect to its position at rest, its x-axis projected form may be written as

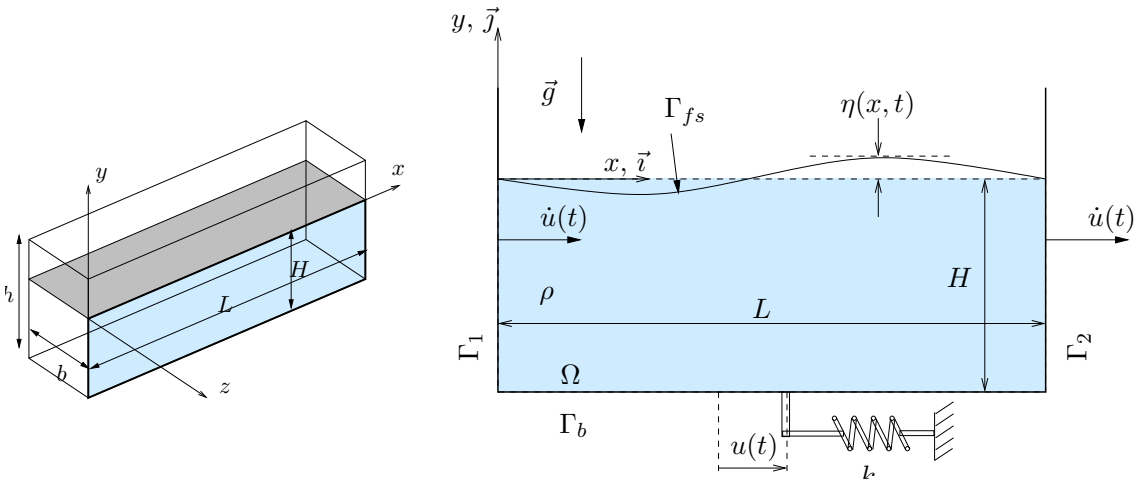

(a) 3D view (b) 2D view

Fig. 1 Definition of the moving, partially filled 2D tank with external rigidity

$$m\frac{d^2u}{dt^2} + ku(t) = f_p(t), \quad \text{with} \quad u(0) = u^0 \text{ and } \dot{u}(0) = 0, \tag{1}$$

where m and k respectively denote the empty tank mass and the rigidity associated to the attachment of the tank to its environment. The f_p term, obtained from the integral of the pressure on the two internal faces Γ_1 and Γ_2, is the pressure effect acting on the tank

$$f_p(t) = f_{p,1}(t) + f_{p,2}(t) = b\int_0^H (p_2(y,t) - p_1(y,t))\,dy = -m_{add,f}\frac{d^2u}{dt^2}, \tag{2}$$

where b is the tank width and $m_{add,f}$ denotes the fluid added mass term.

2.2 Potential fluid model

Potential fluid flow analysis is based on the assumptions of an incompressible and irrotational (inviscid) fluid flow. Under these assumptions it is possible (Mottelet 2000) to define a velocity potential function ψ that explicitly takes the tank motion into account

$$\vec{\nabla}\psi = \vec{V} + \dot{u}(t)\vec{i} = \vec{\nabla}\Phi + \dot{u}(t)\vec{\nabla}\psi_0, \text{ and then } \psi = \Phi + \dot{u}(t)\psi_0, \tag{3}$$

where $\vec{V}(x,y,t)$ denotes the local fluid flow velocity and is relative to the tank velocity $\dot{u}$. The potential function has been split into two components Φ and ψ_0, respectively related to the relative fluid velocity and to the wall tank velocity $\dot{u}$. Combining this with the two assumptions yields the classical Poisson equation

$$\Delta\psi = 0 \text{ in } \Omega. \tag{4}$$

2.2.1 Free surface equation

This results from combining a dynamic condition (pressure) and a kinematic condition (velocity). The use of the non-stationary form of Bernoulli's equation on the free surface Γ_s gives

$$g\eta + \frac{1}{2}\left(\vec{\nabla}\psi\right)^2 + \dot{\psi} = 0 \text{ on } \Gamma_{fs},$$

where η and g respectively denote the free surface elevation and the acceleration of gravity. Neglecting the nonlinear kinetic term $\left(\vec{\nabla}\psi\right)^2$ with regards to the potential one, we easily obtain the dynamic boundary condition

$$g\eta + \dot{\psi} = 0 \quad \Rightarrow \quad \eta = -\frac{\dot{\psi}}{g} \text{ on } \Gamma_{fs}. \tag{5}$$

With this assumption, the validity of this model is voluntarily restricted to a linear behaviour of the free surface. The equality between the vertical component of the fluid velocity and the time derivative of $\eta(x,t)$ leads to the kinematic boundary condition

$$\dot{\eta} = \vec{\nabla}\psi.\vec{n} = \frac{\partial\psi}{\partial n} \text{ on } \Gamma_{fs}.$$

Combining the two equations above finally yields the free surface equation

$$\ddot{\psi} + g\frac{\partial\psi}{\partial n} = 0 \text{ on } \Gamma_{fs}. \tag{6}$$

2.2.2 Boundary conditions on the walls

The two vertical walls $\Gamma_{1,2}$ are assumed to rigid but movable at velocity $\dot{u}$

$$\frac{\partial \psi}{\partial n} = -\dot{u}(t) \text{ on } \Gamma_1 \text{ and } \frac{\partial \psi}{\partial n} = \dot{u}(t) \text{ on } \Gamma_2, \tag{7}$$

where $\vec{n}$ always denotes a normal exterior vector. The boundary condition for the bottom part is

$$\frac{\partial \psi}{\partial n} = 0 \text{ on } \Gamma_b. \tag{8}$$

To summarize, the potential fluid flow problem is governed by the complete set of Eqs. (4), (6), (7) and (8).

3. Numerical models

3.1 Structure model

The time resolution of the left term of the Eq. (1) is here obtained using a Newmark-Wilson finite difference (Dhatt *et al.* 2012) scheme. It is based on the following time series expansions on u and $\dot{u}$

$$u^{n+1} = u^n + \Delta t \dot{u}^n + \frac{\Delta t^2}{4}(\ddot{u}^n + \ddot{u}^{n+1}), \quad \dot{u}^{n+1} = \dot{u}^n + \frac{\Delta t}{2}(\ddot{u}^n + \ddot{u}^{n+1}), \tag{9}$$

The indexes n and $n+1$ correspond to the times t and $t + \Delta t$. We easily deduce the variation $\Delta u = u^{n+1} - u^n$ from

$$\left(\frac{4m}{\Delta t^2} + k\right) \Delta u = f_p^n - k u^n + m\left(\frac{4}{\Delta t}\dot{u}^n + \frac{1}{4}\ddot{u}^n\right). \tag{10}$$

It should be pointed out that the fluid load term f_p, resulting from fluid pressure integration on the two internal faces Γ_1 and Γ_2 of the tank, is here computed at time step n because of the partitioned nature of the considered coupling scheme.

3.2 Potential fluid model model: condensing the free surface problem

The idea here is to condense the 2D problem by projecting it onto the 1D free surface and in so doing to reduce significantly the size of the problem to be solved (Morand and Ohayon 1995). Let φ denote the potential function attached to the free surface, such that $\varphi = \psi|_{\Gamma_{fs}}$. In the context of finite element (Dhatt *et al.* 2012) solving approach, the weak form of Eq. (6) is given by

$$\int_{\Gamma_{fs}} \delta\varphi \left(\ddot{\varphi} + g\frac{\partial \psi}{\partial n}\right) ds = 0 \quad \forall\, \delta\varphi(x), \tag{11}$$

where $\delta\varphi(x)$ is an arbitrary test function. The key to condensing the problem in this way is to relate the derivative term to the weak form of Eq. (4) after an integration by parts that naturally lets the boundary conditions appear (Eqs. (7) and (8))

$$\iint_{\Omega} \vec{\nabla}\delta\psi.\vec{\nabla}\psi dx dy + \int_{\Gamma_1} \delta\psi\, \dot{u}(t)\, ds - \int_{\Gamma_2} \delta\psi\, \dot{u}(t)\, ds - \int_{\Gamma_{fs}} \delta\psi \frac{\partial \psi}{\partial n} ds = 0 \quad \forall\, \delta\psi(x,y).$$

Isolating the last integral term, we can write

$$\int_{\Gamma_{fs}} \delta\varphi g \frac{\partial \psi}{\partial n} ds = < \delta\psi > \left([K_\psi]\{\psi\} - \{F_\psi\} \right),$$

where $\{\psi\}$ is the global vector for all degrees of freedom (abbr. *dof*) corresponding to the 2D-domain. The splitting of the potential function into two components (see Eq. (3)) can be extended to all *dof* such that

$$\{\psi\} = \{\Psi\} + \{\psi_o\}\dot{u} = [D]\{\varphi\} + \{\psi_o\}\dot{u},$$

where $\{\varphi\}$ is the global vector for all *dof* corresponding to the free surface. The condensing matrix $[D]$ acts as a transfer matrix such that

$$[K_\varphi] = [D]^T[K_\psi][D] \quad \text{and} \quad \{F_\varphi\} = [D]^T\{F_\psi\},$$

and is obtained in only one shot from the resolution of

$$\Delta\Psi = 0 \text{ in } \Omega, \quad \Psi = \varphi \text{ on } \Gamma_{fs}, \quad \frac{\partial \Psi}{\partial n} = 0 \text{ on } \Gamma_b \cup \Gamma_1 \cup \Gamma_2.$$

Finally, the finite element discretization of Eq. (11), based on a linear two-node element, gives the set of equations

$$[M_\varphi]\{\ddot{\varphi}\} + [K_\varphi]\{\varphi\} = \{F_\varphi\}. \tag{12}$$

Because of the condensing approach, $[K_\varphi]$ and $\{F_\varphi\}$ are a full matrix and vector. This system is completed by initial conditions $\{\varphi\} = \{\dot{\varphi}\} = \{0\}$ corresponding to a free surface initially at rest.

In order to illustrate the condensing process, we show in Fig. 2(a) the volume of fluid in a non rectangular tank that has been condensed to only keep the free surface nodes (Fig. 2(b)).

3.3 Validation cases for the fluid model

3.3.1 Constantly accelerating tank

This example is based on the classical solution for the slope of the free surface in the case of a constantly accelerating tank. The exact slope is given by $\theta = -\ddot{u}/g$. We consider the two directions

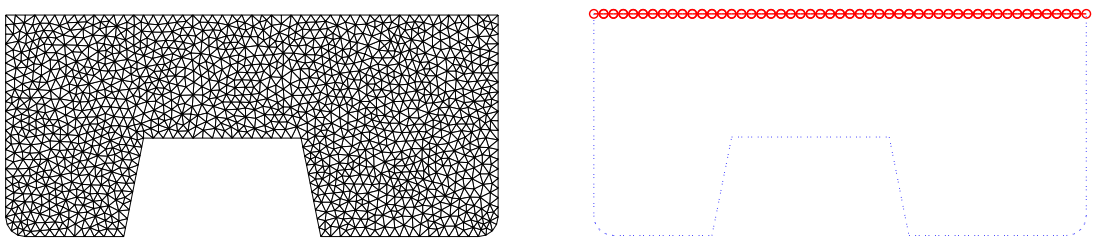

(a) Initial fluid mesh (b) Mesh Condensed to free surface nodes

Fig. 2 Free surface condensing process to reduce CPU time

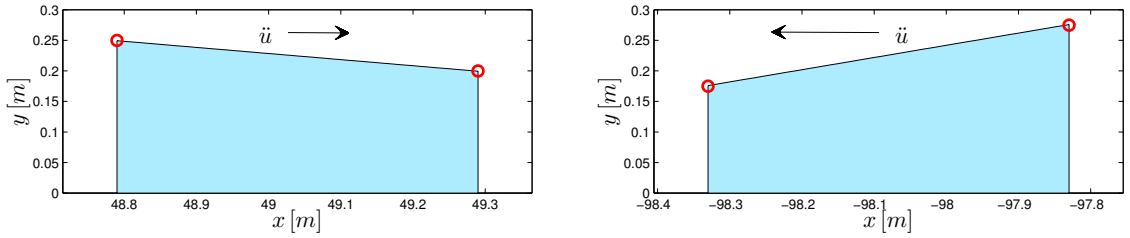

(a) $\ddot{u} = +0.1$ m/s^2, $u(10\,s) = 49.05$ m (b) $\ddot{u} = -0.2$ m/s^2, $u(10\,s) = -98.1$ m

Fig. 3 Free surface slope resulting from a constantly accelerating tank

Table 1 Mesh properties ($L = 0.5$ m, $H = 0.225$ m, $b = 1$ m)

Parameter	Δx [m]	Nodes	T3 element	L2 element	Number of *dof*
Mesh I	0.01	1561	3120	50	51
Mesh II	0.005	5949	11896	100	101

for $\ddot{u} = +0.1$ m/s^2 and $\ddot{u} = -0.2$ m/s^2 respectively. Figs. 3(a)-(b) illustrate the two cases. The circle symbols help to locate the exact position at the two extremities of the free surface.

Mesh properties are summarized in Table 1, where T3 and L2 respectively denote a triangular 3-node element and a linear two-node element. Mesh I is here considered and we recall here that thanks to the condensing approach exposed in § 3.2, the global size of the problem to solve is here limited to only 51 dof!

The FEM solution requires the introduction of a damping matrix (equal to $[K_\varphi]$) in order to rapidly converge to the stationary solution, limiting oscillations that naturally appear for the transient phase. A total number of 100 steps are required for a time step $\Delta t = 10^{-1} s$.

3.3.2 Sloshing response of a partially filled tank for a soft braking: comparison with experimental data

This last example permits to compare the potential model with 3D experiments from A. Brandely (Brandely and Lefrançois 2016) and extracted from a rigid and partially filled tank that undergoes a *soft* braking. The experiment is based on a rigid tank placed on an inclined test bench where the motion results only from gravity effect. A belt is used to stop the tank motion and helps to simulate a real car breaking effect. More details of the experiments may be found in (Brandely and Lefrançois 2016).

Dimensions of the tank are $L = 0.5$ m, $b = 0.35$ m and $h = 0.3$ m (see Fig. 1(a)). The acceleration $\ddot{u}(t)$ along the $x-$axis is extracted from experiments and injected in the fluid solvers as a transient boundary condition for the tank walls. This comparison essentially points out the period of impact resulting from the complete stop of the tank. A viscous CFD simulation based on a VOF (Volume Of Fluid) approach with Star-CCM+ is also considered for comparison.

Results are given in Fig. 4. The upper graph is the acceleration profile imposed to the tank. Forces integrated on both walls (according to Eq. (2)) are plotted in the lower part respectively for the potential model, Star-CCM+ and experiments.

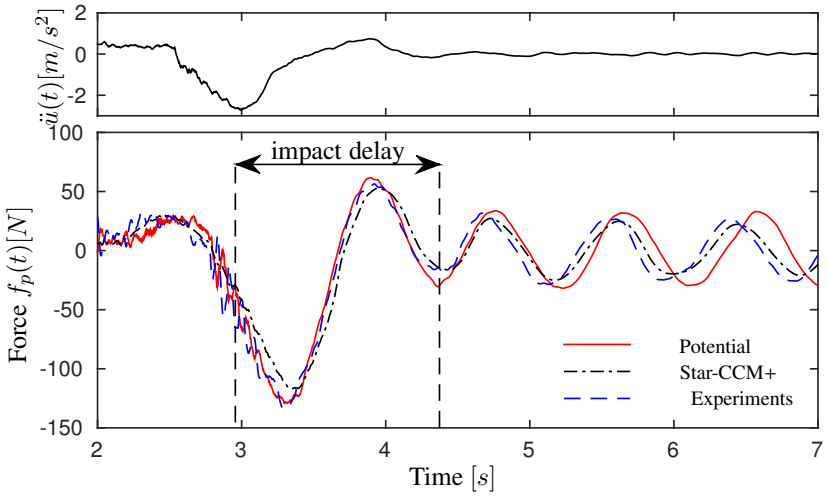

Fig. 4 Comparison between the potential fluid model and experiments: soft braking of a partially filled tank

Close to the impact, the solution obtained from the potential approach (straight line) is in a very good agreement with experiments (dashed line), as well as for the force amplitude than the impact delay. After the complete stop of the tank, we observe a constant amplitude oscillation and a slightly higher period of oscillation. These results are not suprising and respectively due to the absence of viscosity in the model and to its linear behaviour. Concerning the CPU time required by both numerical approaches, it takes about one minute for the potential model (Matlab), whereas it takes several days for the viscous VOF method (Star-CCM+).

3.4 Strongly coupled partitioned scheme

Eq. (1) is the fluid-structure interaction equation. The partitioned approach consists in allocating each of the terms to the left and right of the equals sign to its own dedicated solver. The staggered nature of the coupling scheme means that both terms are successively solved in 4 steps, as illustrated in Fig. 5.

Indices n and $n+1$ correspond to time steps t and $t+\Delta t$ respectively. In order to reduce

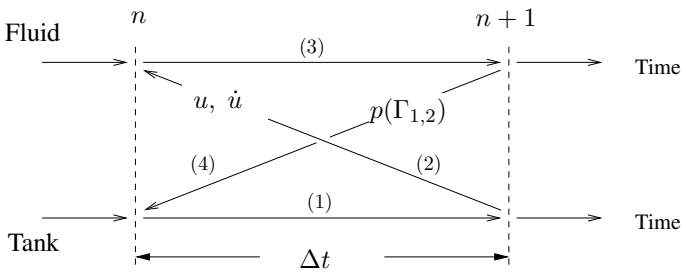

Fig. 5 Partitioned and staggered coupling scheme

the discrepancy between a tank motion computed at $n+1$ from a pressure given at time n, and consequently to reinforce the coupling, an enclosed iterative procedure is then added inside the temporal loop. The general algorithm (Algorithm 1) is based on an iterative loop (i) enclosed in a time loop (n). Each equation is then modified, with $n+1$ replaced by $i+1$.

Algorithm 1 General partitioned algorithm

Require: $u(0),\ \dot{u}(0) \rightarrow \ddot{u}(0)$
$u^n \leftarrow u(0), \dot{u}^n \leftarrow \dot{u}(0), \ddot{u}^n \leftarrow \ddot{u}(0)$
Require: $p_1(y,0),\ p_2(y,0)$
for $n = 1$ to $nstep$ **do**
  for $i = 1$ to $niter$ **do**
    ———————— *Dynamic tank part*
    $f_p^i \leftarrow p(\Gamma_{1,2})$
    $\Delta u \leftarrow$ Eq.(10)
    $\dot{u}^{i+1} \leftarrow$ Eq.(9)
    ———————— *Fluid part*
    $\varphi^{i+1} \leftarrow$ Eq.(12)
    $p(\Gamma_{1,2}) \leftarrow$ Eq.(13)
  end for
  $u^{n+1} = u^n + \Delta u$
  $\dot{u}^{n+1},\ \ddot{u}^{n+1} \leftarrow$ Eq.(9)
  $u^n \leftarrow u^{n+1}, \dot{u}^n \leftarrow \dot{u}^{n+1}, \ddot{u}^n \leftarrow \ddot{u}^{n+1}$
end for

The coupling scheme is based on data passing, so as to update variables common to the two physics. The tank transmits its position u and its velocity $\dot{u}$, whereas the fluid transmits its pressure field acting on the two vertical walls. This pressure field is obtained using the non-stationary form of Bernoulli's equation

$$p(y,t) = -\rho g y - \frac{1}{2}\rho \dot{u}^2 - \rho \frac{\partial \psi}{\partial t} \text{ on } \Gamma_{1,2}.$$

We should point out that the derivative for $\dfrac{\partial \psi}{\partial t}$ is deduced from the material derivative

$$\frac{\partial \psi}{\partial t} = \frac{d\psi}{dt} - \overrightarrow{V_m}.\overrightarrow{V_f},$$

where $\overrightarrow{V_m}$ and $\overrightarrow{V_f}$ respectively denote the local domain velocity and the fluid flow velocity. On both walls they are equal to $\dot{u}$. We then have

$$p(y,t) = -\rho g y + \frac{1}{2}\rho \dot{u}^2 - \rho \frac{d\psi}{dt} \text{ on } \Gamma_{1,2}, \tag{13}$$

where $\dfrac{d\psi}{dt}$ is computed from a finite difference scheme for which the order of accuracy may have an impact on the convergence properties.

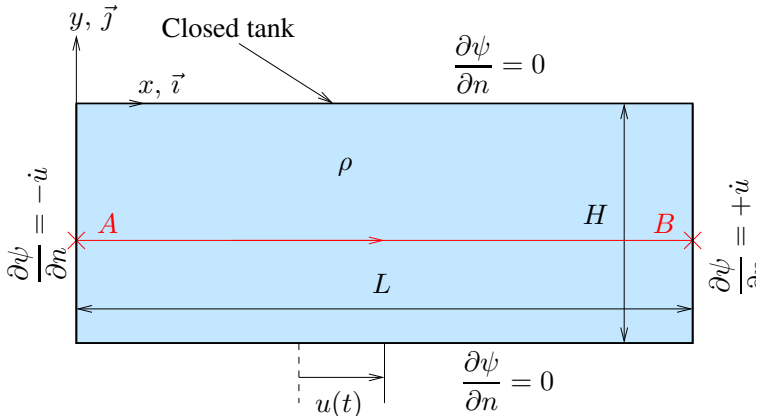

Fig. 6 Particular case of a closed, full tank

4. Added mass effect and corrected coupling scheme

4.1 Particular case of a closed full tank

This particular case of a moving closed tank offers an analytical solution that makes explicit the added mass effect. Moreover, this particular case, illustrated in Fig. 6, represents an extreme case, namely the validation of an FSI where only the mass effect of the fluid interacts with the dynamics of the tank.

The fluid we consider is water ($\rho = 1000$ kg/m^3). The exact solution is obtained directly (PFD form with fluid and tank masses added), but the non-stationary form of Bernoulli's equation allows the pressure force acting on the two vertical walls to be determined. Applying it along the streamline connecting A and B gives

$$p_B - p_A + \rho \left(\frac{\partial \psi_B}{\partial t} - \frac{\partial \psi_A}{\partial t} \right) = 0. \tag{14}$$

Regarding the boundary conditions, the potential function is simply given by

$$\psi(x) = \dot{u}x + b, \tag{15}$$

and then

$$p_B - p_A = \rho \frac{d^2u}{dt^2}(x_A - x_B) = -\rho L \frac{d^2u}{dt^2}.$$

This term is not y-dependent. Consequently and according to Eq. (1), the fluid force term acting on the tank (Eq. (2)) can be rewritten as

$$f_p = (p_B - p_A)bH = -m_{add,f} \frac{d^2u}{dt^2} \quad \text{with} \quad m_{add,f} = \rho bHL = m_f \tag{16}$$

where the fluid added mass term $m_{add,f}$ is, for this particular case, identical to the enclosed fluid mass m_f. Injecting it into Eq. (1) yields the classical and predictable mass-spring form

$$(m + m_f)\frac{d^2u}{dt^2} + ku = 0, \quad \text{with} \quad u(0) = u_o,$$

whose exact solution is

$$u(t) = u_o \cos(\omega_c t), \quad \text{with} \quad \omega_c^2 = \frac{k}{m + m_f}, \tag{17}$$

where ω_c denotes the pulsation of the coupled system.

4.1.1 Convergence analysis of the FSI scheme

From Eqs. (1), (13) and (15), the iterative coupling process is then given by

$$m\ddot{u}^{i+1} + ku^{i+1} = (p_B^i - p_A^i)bH = -m_f \left(\frac{\dot{u}^i - \dot{u}^n}{\Delta t} \right). \tag{18}$$

The term $d\psi/dt$ required for the pressure calculation is here discretized according to a first-order finite difference scheme. Convergence analysis requires it to be rewritten in the form

$$u^{i+1} = f(u^i) \quad \text{with} \quad u^o,$$

for which convergence is ensured if $f(u)$ is continuously differentiable, $|df/du| < 1$ and u^o sufficiently close to the solution. When combined with Eq. (9) taken at iterations $i+1$ and i, Eq. (18) can be rewritten as

$$u^{i+1} = -\frac{m_r}{2 + \Delta t^2 \omega^2/2} u_i + \dots$$

The term $m_r = m_f/m$ is the mass ratio and $\omega = \sqrt{k/m}$ denotes the natural pulsation. The time step Δt can be rewritten as

$$T = N\ \Delta t \quad \text{with} \quad T = \frac{2\pi}{\omega} \quad \text{and then} \quad \Delta t^2 \omega^2 = \frac{4\pi^2}{N^2}.$$

where N denotes the sample of the period T. We then identify

$$f(u^i) = G\ u^i + ... \quad \text{with} \quad G = -\frac{m_r}{2 + 2\pi^2/N^2}. \tag{19}$$

The convergence is then ensured if

$$\left| \frac{df}{du} \right| = |G| < 1 \quad \Rightarrow \quad m_r < 2 \left(1 + \frac{\pi^2}{N^2} \right). \tag{20}$$

Considering a 2nd or 3rd order of accuracy for $d\psi/dt$, respectively given by

$$\left.\frac{d\psi}{dt}^i\right|_{2nd} = \frac{\frac{3}{2}u^i - 2u^n + \frac{1}{2}u^{n-1}}{\Delta t} + \Delta t^2(\dots), \quad \left.\frac{d\psi}{dt}^i\right|_{3rd} = \frac{\frac{11}{6}u^i - 3u^n + \frac{3}{2}u^{n-1} - \frac{1}{3}u^{n-2}}{\Delta t} + \Delta t^3(\dots),$$

we can easily show that the corresponding critical values for m_r are respectively multiplied by $2/3$ and $6/11$. It is to be remarked that increasing the order of accuracy is extremely penalizing for convergence.

Table 2 Parameters for full, closed tank coupling

Parameter	$u_o\,[m]$	$m\,[kg]$	$k\,[N/m]$	$L\,[m]$	$H\,[m]$	$m_f\,[kg]$	$\Delta t\,[s]$	$nstep$	N
Value	0.01	50	10^4	0.5	0.225	112.5	10^{-2}	10	45

Table 3 Critical mass ratio for convergence versus order of accuracy for time discretization

Order of accuracy for $\partial\varphi/\partial t$	1st	2nd	3rd
Critical value fo m_r	2.01	1.34	1.1

4.1.2 Numerical validation and sensitivity to the order of accuracy in time

To validate the predicted results for the effect of mass ratio on convergence, FSI calculations were carried out for the case illustrated in Fig. 6 with different values of m_r. Table 2 summarizes the material properties.

The iterative loop is controlled by the following convergence criterion

$$\varepsilon^i = \left(\sqrt{< \Delta\ddot{u} > \{\Delta\ddot{u}\}}\right)/ndof < 10^{-4} \text{ with } \{\Delta\ddot{u}\} = \{\ddot{u}\}^i - \{\ddot{u}\}^{i-1},$$

where $ndof$ denotes the total number of *dof*. From Eq. (20) and the above remark on orders of accuracy, Table 3 summarizes the predicted limit value of m_r ensuring convergence for orders of accuracy from 1 to 3.

FSI calculations were done in accordance with Algorithm 1 and the number of iterations (mean value) required for convergence is given in Table 4. Each column corresponds to a mass ratio (function of ρ) and each line to an order of accuracy for $d\psi/dt$. The '-' sign denotes a divergence result.

For any order of accuracy, the obtained results are totally in accordance with the predicted critical values of m_r: higher values systematically lead to divergence.

4.2 Corrected staggered scheme with added mass effect

The correction that we introduce to improve the convergence is similar to that described by Lefrançois in (Song *et al.* 2013). It is based on the observation that increasing the inertial term or decreasing the force term will favor the iterative process. The main idea is to add an inertial term on both sides of the equation, function of the added mass, such that

$$m_{add,e}\ddot{u}^{i+1} + \quad m\ddot{u}^{i+1} + ku^{i+1} \approx f_p^i \quad + m_{add,e}\ddot{u}^i. \tag{21}$$

where $m_{add,e}$ denotes an estimate for the real added mass term. The contributions of the left- and right-hand terms are taken at iterations $i+1$ and i respectively. If convergence is reached, $\ddot{u}^i = \ddot{u}^{i+1}$ and the original expression (Eq. (1)) is exactly satisfied.

The convergence analysis of the substitution method applied to Eq. (21) requires the same approach as in §4.1.1. From the general relations of Newmark's scheme (Eq. (9)) it is necessary to isolate

$$\ddot{u}^{i+1} = \frac{4}{\Delta t^2}u^{i+1} + \ldots, \quad \text{and} \quad \ddot{u}^i = \frac{4}{\Delta t^2}u^i + \ldots$$

so as to deduce

$$\left(4(m_{add,e} + m) + \Delta t^2 k\right) u^{i+1} = 4(m_{add,e} - m_{add,f})u^i + \ldots$$

Table 4 Number of iterations for FSI convergence for the non-corrected staggered coupling scheme

m_r	0.225	0.45	0.9	1.08	1.32	1.57	1.91	1.99	2.025
1^{st}order for $\partial\varphi/\partial t$	5	7	11	14	20	33	72	1300	-
2^{nd}order	6	9	22	38	850	-	-	-	-
3^{rd}order	7	11	42	550	-	-	-	-	-

Table 5 Number of iterations for FSI convergence for the corrected staggered coupling scheme

m_r	0.225	0.45	0.9	2.25	4.5	10
1^{st} order for $\partial\varphi/\partial t$	5	6	7	8	8	14
2^{nd} order	4	5	5	6	6	9
3^{rd} order	4	4	5	5	5	6

We then identify a general expression for the amplification coefficient as

$$G = \frac{1}{(1+\pi^2/N^2)}\left(\frac{m_{add,e} - m_{add,f}}{m_{add,e}+m}\right) \quad \text{with} \quad \lim_{m_{add,e}\to\infty} G < 1\,! \tag{22}$$

N denotes the sample of the coupled period $T_c = 2\pi/\omega_c$ with $\omega_c^2 = k/(m_{add,e}+m)$ the coupled pulsation. It is now interesting to study how much the estimated $m_{add,e}$ is required to ensure convergence. This expression clearly shows that precisely estimating the added mass term ($m_{add,e}$) is a key but not only, to ensure convergence whatever the fluid density considered. It also shows that an overestimation will suffice. For the particular case where $m_{add,e} = 0$ (no correction) we recover the situation exposed in §4.1.1.

The same validation as detailed in § 4.1.2 was carried out for the higher mass ratio values shown in the first line of Table 5. We naturally consider $m_{add} = m_f$. Convergence is systematically reached whatever the mass ratio, which confirms the beneficial effect of the correction for the coupling scheme. The FEM solutions perfectly match (not shown here) the predicted coupled solution given by (17) in terms of pressure, displacement and coupled pulsation ω_c. Moreover, the numbers of iterations required are lower than for the classical case. It has also been observed (see Table 5), that increasing the order of accuracy for the term $\partial\varphi/\partial t$ really helps convergence and may have a real impact in reducing the number of iterations required.

Even if the added mass term is exactly known, convergence still requires about 5 iterations. The reason for this is the last term of Eq. (18). Even though it is similar to an acceleration, its time derivative is quite different (first order) from that retained for the inertial term, which is based on the Newmark scheme (second order). Because of this the two terms cannot be combined in a single acceleration term.

4.3 General cases

4.3.1 Added mass estimation

We here consider the case of a flexible structure composed of n *dof* in order to expose the added mass estimation for the general cases. The calculation of the added mass matrix $[M_{add}]$ is based on the assumptions that the fluid flow is inviscid and that convective effects can be neglected with regard to the pressure gradient field. This leads to the classical Poisson equation for the pressure p on the

domain Ω, completed by boundary conditions related to the body parietal accelerations

$$\Delta p = 0 \; \forall \; \vec{x} \in \Omega \text{ with } \vec{\nabla} p.\vec{n} = \rho_f \vec{\ddot{u}}.\vec{n} \text{ on } \partial\Omega_1 \text{ and } \vec{\nabla} p.\vec{n} = 0 \text{ on } \partial\Omega_2. \tag{23}$$

The boundary is dispatched according to movable parts $\partial\Omega_1$ and to fixed parts $\partial\Omega_2$, and $\vec{n}$ denotes the normal vector oriented external to the flow. The calculation of $[M_{add}]$ first requires the computation of the global (or partial) set of N eigenvectors of the structures denoted $\{V_i\}$ such that

$$\{U\} = \sum_{i=1}^{N} a_i \{V_i\}, \quad \text{such as} \quad < V_i > \{V_i\} = 1 \quad \text{and} \quad p = \sum_{i=1}^{N} \ddot{a}_i \mathcal{P}_i, \tag{24}$$

where $\mathcal{P}_i$ is the modal component of the pressure field related to the i^{th} eigenvector of the structure. This, together with Eq. (23), enables the solution of N Poisson equations

$$\Delta \mathcal{P}_i = 0 \quad \forall \; \vec{x} \in \Omega \quad \text{with} \quad \vec{\nabla} \mathcal{P}_i.\vec{n} = \rho_f \vec{V_i}.\vec{n} \text{ on } \partial\Omega_1. \tag{25}$$

Finally, the component $M_{add}(i,j)$ is deduced from

$$m_{add}(i,j) = \oint_{\partial\Omega_1} \mathcal{P}_j \vec{V_i}.\vec{n} ds \quad \text{such that} \quad [m_{add}] = [X]^T [M_{add}][X], \tag{26}$$

where $[m_{add}]$ is the projection of the added mass matrix on the eigenvector base $[X] = [\{V_1\} \ldots \{V_N\}]$. For the considered case (tank) with only one dof, the added mass term is given by a scalar

$$m_{add} = \oint_{\partial\Omega_1} \mathcal{P}_1 \vec{\imath}.\vec{n} ds = \int_{\Gamma_2} \mathcal{P}_1 ds - \int_{\Gamma_1} \mathcal{P}_1 ds. \tag{27}$$

4.3.2 Application to a partially filled tank

We now consider the general case of a tank partially filled with water ($\rho = 1000$ kg/m^3), where L/H defines the aspect ratio of the fluid domain. FSI calculations based on the non-corrected coupling scheme were performed with $L = 0.5$ m and H from 0.05 m to 0.5 m in order to show the convergence limit. Properties are summarized in Table 2. Convergence histories are plotted in Fig. 7(a) for the different aspect ratios L/H and for a third order of accuracy for the time derivative. The total number of steps is 50 and $\Delta t = 10^{-2}$ s.

We clearly see that the number of required iterations dramatically increases for lower aspect ratios. Convergence ceases to be guaranteed for an aspect ratio $L/H < 2.17$. Reducing the order of accuracy (first and second) respectively gives $L/H < 1.5$ and 1.96.

Fig. 7(b) illustrates the beneficial effect of the corrected coupling scheme on convergence for the case $L/h = 2.17$ where the number of iterations required (~ 4) is several orders lower than in the non-corrected case (~ 1500). Calculations with lower aspect ratio values ($L/H = 0.5$ and 0.25) systematically converged with $4 \sim 5$ iterations per time step.

The coupling results for $L/H = 2.22$ are plotted in Fig. 8 for a finer mesh (Mesh II, see Table 1) over total number of 500 steps, with a time step $\Delta t = 0.005$ s. The first plot (a) illustrates the normalized tank displacement with two different x-axes: the bottom x-axis corresponding to a

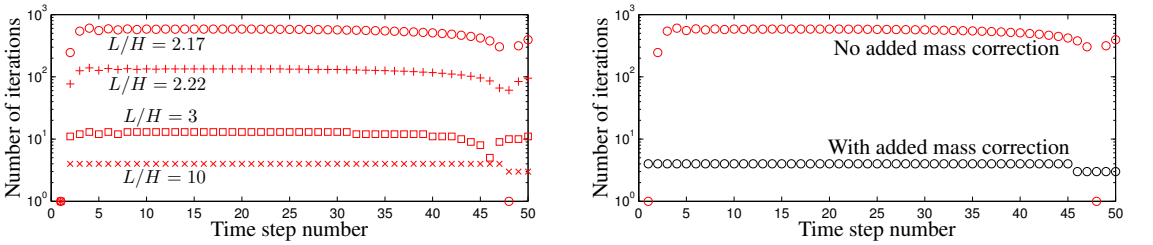

(a) Influence of L/H on convergence (no correction) (b) Comparison with the corrected scheme ($L/H = 2.17$)

Fig. 7 Effect of added mass correction on convergence (water, $m = 50$ kg, order 3)

normalization by the natural tank pulsation ($\omega = 20$ rad/s), and the top x-axis to the coupled pulsation given by Eq. (17) ($\omega_c = 14.01$ rad/s). The time axis is normalized so it can be read as a number of cycles. This plot shows first and foremost that the tank responds with a pulsation close to the coupled pulsation ω_c: a clear sign that the added mass effect pilots the dynamics of the tank, which no longer responds according to its natural pulsation.

Fig. 8(b) illustrates the sloshing mode participation calculated by projecting the free surface force term $\{F_\varphi\}$ onto the Eigenmodes $[\mathcal{X}]$ of the set of Eq. (12) such that the participation coefficient of mode i is given by

$$\alpha_i =< \mathcal{X}_i > \{F_\varphi\}.$$

Because of the initial conditions corresponding to an initial displacement $u(0)$ from its position at rest, only non-symmetric modes (even numbers) participate in the coupling.

Fig. 8(c) illustrates the time histories of the pressure forces acting on the two internal walls of the tank. Both curves are normalized according to the pressure force acting at rest on each wall $f_{p,i}(0) = \rho g H^2/2$. The dashed lines show the forced values for the case of a tank at rest. The tank dynamics may lead to values that are three times the values at rest.

In the absence of a physical damping effect and for a free coupling regime (no forced excitation), the sum of the total energy of the fluid and the tank remains constant over time and equal to the energy resulting from the initial conditions. This energy conservation is one of the key elements that ensure high quality FSI calculations. Fig. 8(d) illustrates the energy exchange between the fluid and the tank, and in particular the global energy conservation. Plots are normalized with the mechanical energy $\mathcal{E}_o$ resulting from the initial tank displacement $u(0)$.

The set of plots in Fig. 9 are snapshots extracted every 25 steps during the coupling process. Arrows indicate the amplitudes and directions of the two pressure forces acting on the tank. The time station t_c for each plot corresponds to the time normalized with regards to the coupled pulsation.

4.3.3 Numerical investigation of the link between the added mass and the aspect ratio L/H

The results given in Fig. 7(a) indicate a strong dependency between the convergence and the aspect ratio L/H of the fluid domain. A numerical investigation was conducted to analyze how the two aspects are linked. The added mass prediction was calculated from Eq. (27) for several cases involving different values for $L \in [0.02,\ 2]$ and $H \in [0.05,\ 2]$ (both in meters). Results are illustrated as a 3D view in Fig. 10 and values are summarized in Table 6 for $L = 0.5$ m and $H \in [0.05,\ 2]$:

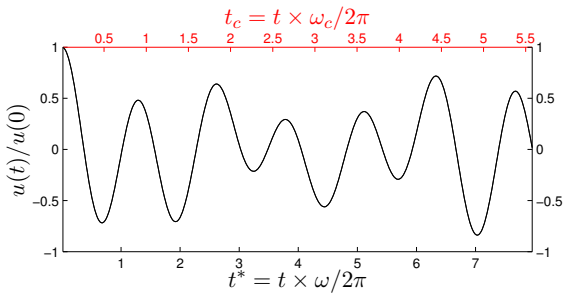

(a) Tank motion $u(t)$ ($\omega_c = 14.01$ rad/s from Eq.(17))

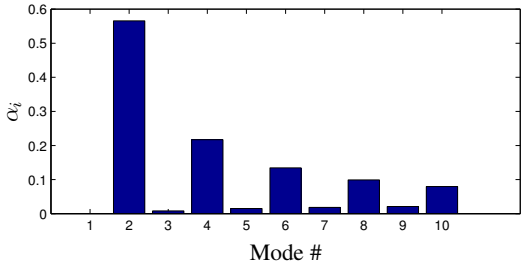

(b) Mode participation

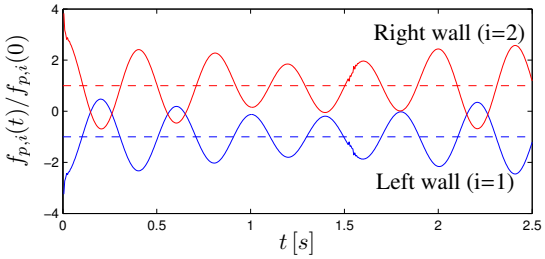

(c) Forces acting on the two walls

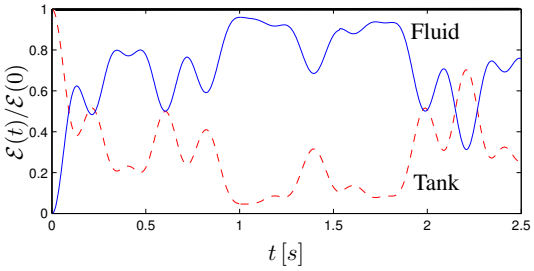

(d) Energy conservation

Fig. 8 FSI coupling: $m = 50$ kg, $k = 2\,10^4$ N/m, $L/H = 2.22$

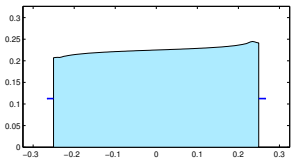

(a) $t_c = 0.27$

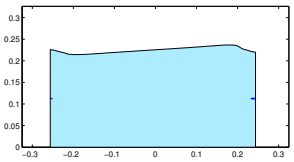

(b) $t_c = 0.55$

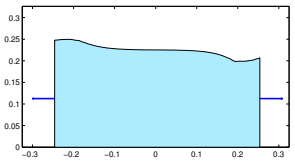

(c) $t_c = 0.83$

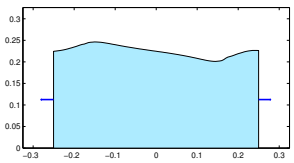

(d) $t_c = 1.11$

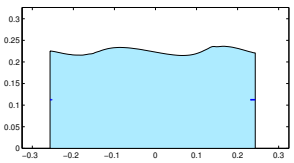

(e) $t_c = 1.39$

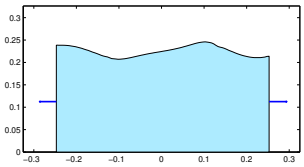

(f) $t_c = 1.67$

Fig. 9 Transient sloshing effect ($m = 50$ kg, $k = 2\,10^4$ N/m, $L/H = 2.22$)

The parameter $H_{eq,add}$ represents the equivalent height of water of the added mass term. It can be seen in Fig. 10 that the added mass term increases for higher values of H (circle symbols and solid line) and decreases for higher values of L (square symbols and dashed line).

Combining both curves to show the aspect ratio L/H gives the superposed results illustrated in

Table 6 Number of iterations for convergence ($L = 0.5$ m) for standard and corrected FSI scheme

H (m)	0.05	0.1	0.2	0.3	0.4	0.5	1	2
m_r	0.5	1	2	3	4	5	10	20
Standard FSI scheme	3	4	20	-	-	-	-	-
Corrected FSI scheme	3	4	5	5	6	6	6	6
$H_{eq,add}$ (m)	0.005	0.02	0.08	0.17	0.26	0.36	0.86	1.86

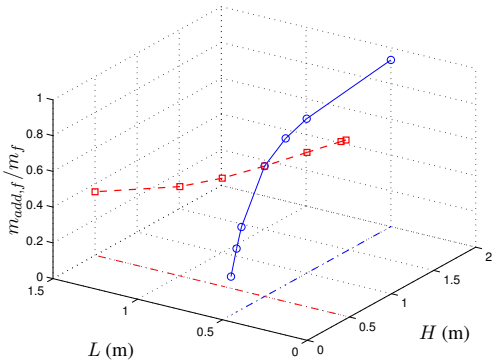

Fig. 10 Sensitivity analysis with regards to m_{add}/m_f ($m = 50$ kg)

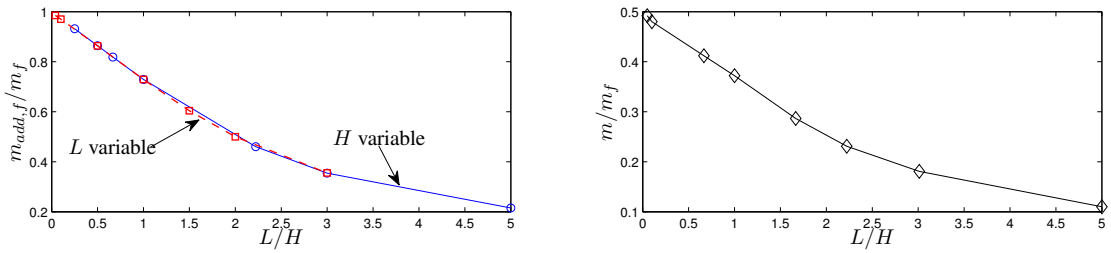

(a) Added mass required for convergence

(b) Tank mass for convergence (classical FSI scheme)

Fig. 11 Added mass effect in relation to the L/H ratio ($m = 50$ kg)

Fig. 11(a), indicating that convergence is controlled by L/H! The lower this aspect ratio, the higher the added mass term, and consequently the greater the difficulty for a non-corrected coupling scheme to converge.

This is unsurprising, given that low aspect ratio values react as a fluid column strongly interacting with the walls, whereas higher values have a longer free surface over which energy can be spread, resulting in less interaction with the walls. To help confirm this interpretation, time histories for fluid and tank energies (respectively denoted by $\mathcal{E}_{FL}$ and $\mathcal{E}_{TK}$) are plotted in Fig. 12(a) and (b) respectively for $L/H = 0.1$ (column shape) and 2.2. Kinetic and potential components are plotted as solid and dashed lines respectively. The most critical case for convergence is for $L/H = 0.1$ and it can clearly be seen that the level of energy exchange is lower than in the other case, and that the potential component for the fluid is quite insignificant in relation to the kinetic component.

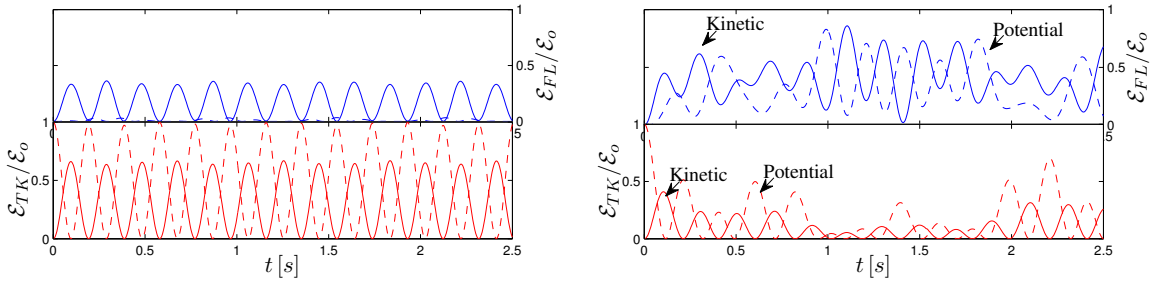

(a) Column shape: $L/H = 0.1$ (b) Rectangular shape: $L/H = 2.22$

Fig. 12 Energies time histories

Table 7 Limit values of the mass ratio for different temporal disretization schemes

Scheme	$\ddot{u}^i$	$\ddot{u}^{i+1}$	Limit for m_r
Newmark	Eq. (9)	Eq. (9)	2
Implicit	$\dfrac{u^i - u^n}{\Delta t}$	$\dfrac{u^{i+1} - 2u^n + u^{n-1}}{\Delta t^2}$	1
Houbolt	$\dfrac{11u^i - 18u^n + 9u^{n-1} - 2u^{n-2}}{6\Delta t}$	$\dfrac{2u^{i+1} - 5u^n + 4u^{n-1} - u^{n-2}}{\Delta t^2}$	$\dfrac{12}{11}$

4.3.4 A mass ratio limit related to the precision order of the time discretization scheme

Fig. 11(b) illustrates the critical mass value for the tank to ensure convergence for a non-corrected coupling scheme. In order to facilitate the comparison with Fig. 11(a), the y-axis is normalized with the fluid mass m_f. The two curves are similar, except for the amplitude. Combining the two shows that the limit convergence is observed for an added mass term $m_{add,f}$ equal to twice the tank mass m, whatever the aspect ratio considered! Higher tank mass values will converge, whereas lower values will diverge (numerically confirmed). This limit ratio is linked to the convergence criterion given by Eq. (20). Indeed, replacing m_f by $m_{add,f}$ for a general case, this explicitly stipulates a limit approximately equal to 2! Even if the criterion is theoretically valuable for a closed, full tank, for open tanks with small displacements, the potential function ψ remains quite close to the particular solution given by Eq. (15). This ratio limit of 2 is then the signature of the Newmark-Wilson scheme used to discretize the tank acceleration. This observation can easily be extended to other classical time discretization schemes. The mass ratio limits for two other schemes are compared in Table 7 with the predicted value for the Newmark-Wilson scheme.

5. Conclusions

This paper presents a corrected version of a strongly coupled partitioned FSI scheme for studying the sloshing effect in a partially filled rectangular tank. It proves that in the particular case of a closed, full tank, the iterative convergence of a classical FSI partitioned scheme ceases to be guaranteed once the mass ratio (fluid mass divided by tank mass) exceeds a predictable value. This value is

directly linked to the signature of the scheme used to discretize the tank acceleration. Correcting the FSI scheme in counteracting the penalizing effect of the added mass, allows convergence to be ensured whatever the mass ratio. For the general case of lightly filled rectangular tanks, this scheme significantly reduces the number of iterations required for convergence in low-density cases that already converge, and ensures convergence in cases where the classical FSI scheme fails to converge. A sensitivity analysis reveals the direct relation between the convergence property and the aspect ratio: the lower the aspect ratio, the higher the added mass term, and consequently the greater the difficulty for a non-corrected coupling scheme to converge. Future work will take account of complex geometric tank shapes and flexible walls. This study will be completed by a comparison with experimental data (PIV analysis under progress).

Acknowledgements

Some of this work benefited from the support of PILCAM2 (Plateforme Inter-Laboratoires de CAlcul Distribués) computer resources, financed as part of an ANVAR support, as well as from support by the Heudiasyc and Roberval laboratories (at Université de Technologie de Compiègne in France).
The authors wish to thank everyone at Inergy Automotive Systems France for the support they provided.

References

Baek, H., Karniadakis, G.E. (2012), "A convergence study of a new partitioned fluid-structure interaction algorithm based on fictitious mass and damping", *J. Comput. Phys*., **231**(2), 629-652.

Brandely, A. and Lefrançois, E. (2015), "A numerical investigation of the added mass effect due to fluid-structure coupling in a rectangular tank", *VI International Conference on Computational Methods for Coupled Problems in Science and Engineering*, 18 - 20 May 2015, Venice, Italy.

van Brummelen, E.H. (2009), "Added mass effects of compressible and incompressible flows in fluid-structure interaction", *J. Appl. Mech*., **76**(2), 021206-7.

Chiba, M., Chiba, S. and Takemura, K. (2013), "Coupled hydroelastic vibrations of a liquid on flexible space structures under zero-gravity-Part I. Mechanical model", *Coupled Syst. Mech*., **2**(4), 303-327.

Dhatt, G., Touzot, G. and Lefrançois, E. (2012), *Finite Element Method*, Wiley-ISTE.

Felippa, C.A., Park, K.C. and Farhat, C. (2001), "Partitioned analysis of coupled mechanical systems", *Comput. Meth. Appl. Mech. and Eng*., **190**(24), 3247-3270.

Fernández, M.A., Gerbeau, J.-F. and Grandmont, C. (2005), "A projection semi-implicit scheme for the coupling of an elastic structure with an incompressible fluid", *Int. J. Numer. Meth. Eng*., **69**(4), 794-821.

He, T. (2015), "Partitioned coupling strategies for fluid-structure interaction with large displacement: Explicit, implicit and semi-implicit schemes", *Wind Struct*., **20**(3), 423-448.

Idelsohn, S.R., Del Pin, F., Rossi, R. and Oñate, E. (2009), "Fluid-structure interaction problems with strong added-mass effect", *Int. J. Numer. Meth. Eng*., **80**(10), 1261-1294.

Kassiotis, C., Ibrahimbegovic, A. and Matthies, H. (2010), "Partitioned solution to fluid-structure interaction problem in application to free-surface flow", *Eur. J. Mech., Part B: Fluids*, **29**(6), 510-521.

Kassiotis, C., Ibrahimbegovic, A., Niekamp, R. and Matthies, H. (2011), "Partitioned solution to nonlinear fluid-structure interaction problems. Part I: implicit coupling algorithms and stability proof", *Comput. Mech*.,

47, 305-323.

Keivani, A., Shooshtari, A. and Aftabi Sani, A. (2014), "Forced vibration analysis of a dam-reservoir interaction problem in frequency domain", *Coupled Syst. Mech.*, **3**(4), 385-403.

Khezzar, L., Seibi, A.C. and Goharzadeh, A. (2009), "Water sloshing In rectangular tanks âĂŞ An experimental investigation & Numerical simulation", *Int. J. Eng.*, **3**(3), 1-11.

Liu, D. and Lin, P. (2009), "Three-dimensional liquid sloshing in a tank with baffles", *Ocean Eng.*, **36**(2), 202-212

Morand, H.J.-P. and Ohayon, R. (1995), *Fluid-Structure Interaction: Applied Numerical Methods*, Wiley.

Mottelet, S. (2000), "Controllability and stabilization of a canal with wave generators", *SIAM J. Control Optimiz.*, **38**(3), 711-735.

Nagashima, T. and Tsukuda, T. (2013), "Seismic response analysis of an oil storage tank using Lagrangian fluid elements", *Coupled Syst. Mech.*, **2**(4), 389-410.

Raj, R.T.K., Bageerathan, T. and Edison, G. (2014), "Design of fuel tank baffles to reduce kinetic energy produced by fuel sloshing and to enhance the product life cycle", *ARPN J. Eng. Appl Sci.*, **9**(3).

Raouf A. Ibrahim (2005), *Liquid Sloshing Dynamics: Theory and Applications*, Ed. Cambridge.

Song, M., Lefrançois, E. and Rachik, M. (2013), "Development of a partitioned algorithm for fluid-structure coupling with no fluid density dependency", *Comput. Fluids*, doi: 10.1016/j.compfluid.2013.05.022.

Sy, S. and Murea, C.M. (2012), "Algorithm for solving fluid-structure interaction problem on a global moving mesh", *Coupled Syst. Mech.*, **1**(1), 99-113.

Veldman, A.E.P., Gerrits, J., Luppes, R., Helder, J.A. and Vreeburg, J.P.B. (2007), "The numerical simulation of liquid sloshing on board spacecraft", *J. Comput. Phys.*, **224**(6), 82-99.

Wachowski, C., Biermann, J.-W. and Schala, R. (2010), "Approaches to analyse and predict slosh noise of vehicle fuel tanks", *Proceedings, ISMA2010.*

Wang, W., Li-xiang, Z., Yan, Y. and Guo, Y. (2012), "Combined multi-predict-correct iterative method for interaction between pulsatile flow and large deformation structure", *Coupled Syst. Mech.*, **1**(4), 361-379.

AI